A Comparative Study on Frequency Scanning Techniques for Stability Assessment in Power Systems Incorporating Wind Parks

Keijo Jacobs, Younes Seyedi, Lei Meng, Ulas Karaagac, and Jean Mahseredjian

***Abstract*--Modern power grids incorporating inverter-based resources (IBRs) may be liable to persistent oscillations and instability incidents, which jeopardize the reliable operation of the power system. Due to the high number and the complexity of the involved components, an analytical stability assessment of modern power grids is infeasible. A viable approach is the impedance-based stability analysis (ISBA) using impedances extracted from manufacturer-specific electro-magnetic transient (EMT) models via frequency scanning. This paper reviews the EMT-level positive-sequence, *dq*-frame and *αβ*-frame frequency scanning techniques and compares their computational efficiencies. The impact of the model reference frame on IBSA precision is also examined on two test cases: I - a full-size converter (FSC)-based wind park (WP) interacts with transmission grid in the super-synchronous frequency range; II - a doubly-fed induction generator (DFIG)-based WP interacts with transmission grid in the sub-synchronous frequency range. Among the compared techniques, ISBA using *dq*-frame impedance models features the highest accuracy. However, IBSA using positive-sequence or *αβ*-frame impedance models is sufficiently accurate. The computational speed of the ps-scan is fastest among the presented techniques. Using *αβ*-frame models has the slowest computational speed and is, therefore, is not recommended.**

Keywords: **Controller interactions, converter, impedance-based stability analysis, wind parks**

I. Introduction

The utilization of renewables, e.g., wind and solar energy, in power systems has increased over the past few years across the globe [1]. The integration of high-capacity wind parks (WP) can bring about major issues related to harmonics, power quality, fault ride-through capability, and stability [2]. WPs are liable to stability issues where controller interactions may lead to oscillations in the sub- or super-synchronous frequency range [3]. Furthermore, it is known that the grid impedance significantly affects the performance of the controllers in grid-connected converters [4]. Oscillation incidents are adverse to the safe operation of the grid [5], and thus should be detected and mitigated in the design phase [6].

To address the above challenges, attempts to detect oscillations and predict stability have been made for systems with doubly-fed induction generator (DFIG) and full scale converter (FSC) WPs [7, 8, 9, 10]. WPs are complex systems with numerous mechanical and power electronic components, controllers, and non-linear dynamics e.g., phase-locked loops (PLLs), limiters, etc. [11]. Therefore, the analysis of controller interactions and stability prediction for such systems is not straightforward. To reduce complexity and computational burden, two methods are commonly applied: state-space modelling using Eigenvalue analysis, and impedance-based modelling using Bode- or Nyquist plots [12].

State-space analysis (SSA) requires detailed knowledge of the converters and their controls. Furthermore, the derivation of the state-space equations remains unpractical for large and complex power systems. Additionally, the model must be reformulated for each structural change.

In impedance-based stability analysis (IBSA) grid components or sections are modelled by impedances and admittances [13]. A system can be divided into source and load (e.g., converter and grid) and brought into feedback form, as illustrated in Fig. 1. Their interaction can then be studied via stability criteria [14, 15, 16].

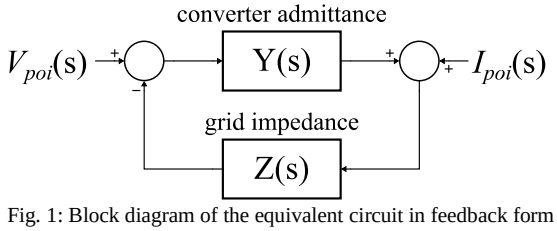

Fig. 1: Block diagram of the equivalent circuit in feedback form

Power electronic converters include non-linear elements (e.g., power semiconductor devices) and non-linear control functions (e.g., current limiters). Therefore, IBRs need to be linearized for a specific operation point. The analytic formulation of frequency-dependent impedance models is tedious and requires detailed knowledge of the modelled

Funding Details to be added for final submission.

K. Jacobs (keijo.jacobs@polymtl.ca), Y. Seyedi (keijo.jacobs@polymtl.ca) and J. Mahseredjian (jean.mahseredjian@polymtl.ca) are with the Department of Electrical Engineering, Polytechnique Montreal, Montreal H3T1J4, Canada. L. Meng (clare-lei.meng@connect.polyu.hk) and Ulas Karaagac (ulas.karaagac@polyu.edu.hk) are with The Hong Kong Polytechnic University, Kowloon, Hong Kong.

Paper submitted to the International Conference on Power Systems Transients (IPST2023) in Thessaloniki, Greece, June 12-15, 2023.

component [17, 18]. An alternative method is frequency scanning. Frequency scanning extracts the impedance model from EMT models [19], hardware-in-the-loop setups, or real-world hardware [20]. One advantage of frequency scanning is that no knowledge of model-internal parameters is required, meaning that it can be applied to proprietary black-box models.

Different types of frequency scanning techniques have been developed: The impedance model can be obtained in positive-sequence [5, 21, 22], synchronously rotating *dq*-frame [20, 22, 23, 24], or the stationary *αβ*-frame [25] (ps-scan, *dq*-scan and *αβ*-scan, respectively). The ps-scan is a single input single output (SISO) model, whereas *αβ*- and *dq*-scan are multiple input multiple output (MIMO) models. Regardless of the type of scan, the main concept is to inject perturbations and observe the systems' response under specific operating conditions. The scanning techniques differ in their computational burden and accuracy. It is thus crucial to investigate and compare the performance of the different scanning techniques.

This paper presents a comprehensive study on existing frequency scanning techniques for IBSA. The ps, *dq*, and *αβ*-scans are reviewed, and their key aspects are discussed and evaluated based on EMT simulations for realistic benchmarks that involve DFIG and FSC WPs. Prediction reliability, stability margin, oscillation frequency estimation, and the simulation time are investigated.

II. Frequency Scanning and Stability Analysis

In the following it is described how to obtain the impedance models via frequency scanning in different reference frames, and how to analyze the stability of the system.

A. Frequency Scanning of EMT Models

The converter subsystem, i.e., the WP, is a non-linear system since it contains power electronic devices, control, and non-linear protection functions. The grid subsystem itself can be a large-scale non-linear system with many converters, e.g., power grids that employ high-voltage direct current (HVDC), photovoltaic and WP systems. These systems must be linearized for a given operation point, which enables the application of small-signal analysis methods.

Time-domain EMT simulations in conjunction with frequency scanning can be used to measure and estimate the impedance models. The steady-state values of the are obtained through load-flow studies for the specified operating conditions. Perturbation signals at one, or multiple, frequencies are superposed on the steady state and the component's response is measures to generate the impedance model. The procedure is shown in Fig. 2 and explained in detail in the following.

The perturbation properties, e.g., frequency, shape [26], and amplitude are parameters of the procedure. Stepwise perturbation signals should be avoided since abrupt disturbances may trigger non-linearities in some cases. A common practice to circumvent this issue is to multiply the perturbations with a limited ramp signal [23].

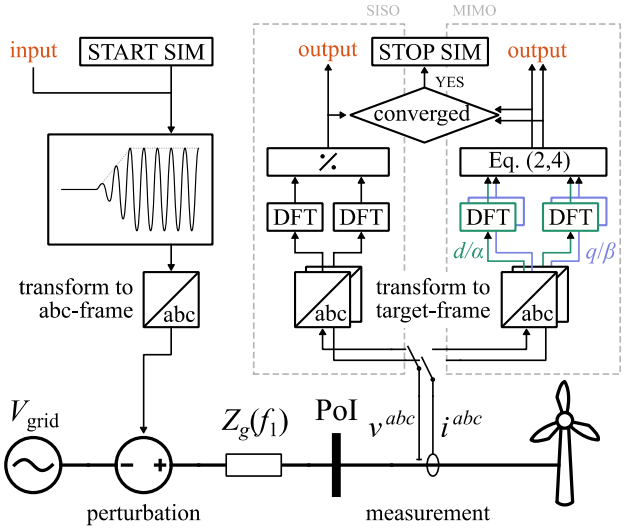

Fig. 2: Frequency scan using voltage perturbation in EMT time-domain model for SISO and MIMO impedance extraction.

Either voltage or current perturbation can be used for scanning grid following IBRs. In principle, both methods yield virtually the same result and accuracy. However, a proper comparison exceeds the scope and page limitations of this paper and only voltage perturbation has been applied for the presented results. The following fundamental differences should be noted:

- Voltage perturbation is connected in series with the grid voltage; therefore, the perturbation signal is superposed on the system voltage.
- Current perturbation is injected into the POI node. A fraction of the perturbation current flows into the grid. This decreases the effective perturbation amplitude with which the converter is perturbed, which in return might affect the accuracy. In extreme cases, for example if the grid impedance is much smaller than the WP, this might affect the operation point of the studied system.

The voltage and current responses are measured at the POI, and the measurements are transformed into the specified reference frame. The impedance/admittance of the subsystem is calculated using a specific frequency component of the measurement, which is computed by a discrete Fourier transform (DFT). To avoid spectral leakage in the DFT, the length of the data segments should span an integer number of the cycles of the fundamental, perturbation, and any coupling frequency [27]. In the presence of measurement noise and harmonics, the calculated impedance parameters may show variations over the time. Therefore, in the last step, a convergence test verifies that the variations of the impedance magnitude and phase angle are negligible. Subsequently, the impedance parameters are saved for post-processing.

The process is repeated in discrete frequency intervals for the range of interest. In this paper the range $[0, 2f_1]$ Hz is scanned in 1 Hz intervals, where f_1 denotes the fundamental frequency.

The grid-side scan can be performed with the same procedure. However, if the grid model is very large and contains other IBRs, this might lead to very long simulation

times. In the presented case, the grid contains only passive linear elements and can be scanned via a phasor domain frequency scanning tool [28] with negligible simulation time.

B. Frequency Scanning in Different Reference Frames

Depending on the chosen reference frame the dimension of the obtained frequency-dependent model may vary. A positive-sequence impedance model is single-input single-output (SISO), whereas *dq* and *αβ* impedance models are multiple-input multiple-output (MIMO). The scanning procedure for all three presented methods is equivalent. While the extraction of a SISO impedance can be done with one scan, a MIMO impedance requires a separate perturbation of each axis and subsequent measurement, as illustrated in Fig. 3. Each EMT simulation is represented by the procedure in Fig. 2.

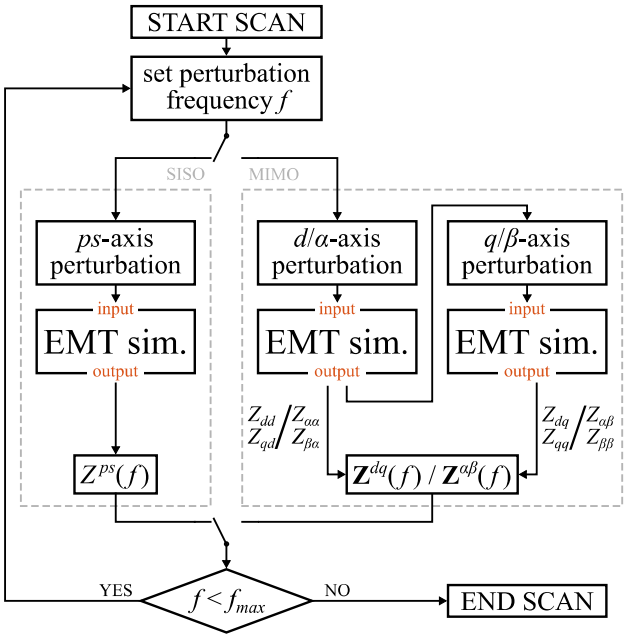

Fig. 3: Generic procedure of frequency scanning for SISO and MIMO impedance extraction (complements Fig. 2 connecting to input and output).

1) Positive Sequence Frequency Scanning

The ps-scan is widely used for impedance extraction of WPs connected to series-compensated transmission systems [5]. For this scanning method, sinusoidal perturbation signals are applied in the sequence domain, and the impedance of the converter subsystem is derived based on the positive sequence components of the voltage and current signals at the POI. The frequency-dependent impedances of the grid and the converter subsystems are denoted by $Z_g^{ps}(f)$ and $Z_c^{ps}(f)$, respectively.

2) dq-Frame Frequency Scanning

The *dq*-scan extracts the small-signal transfer functions that relate the input currents (voltages) to the output voltages (currents) in the synchronous rotating reference frame. In this scanning method, the perturbation signals are applied on *d*- or *q*-axis in two separate simulation runs. For each simulation run, the measured voltages and currents are transformed into the *dq*-frame and the target frequency component is extracted via DFT for both axes. The impedance or admittance is then calculated for two of the four required model elements. The impedance or admittance in the *dq*-frame are 2 × 2 MIMO models.

The grid-side impedance in *dq*-frame can be transformed from the phasor-domain-scan via

$$\mathbf{Z}_g^{dq}(f) = \mathbf{T}_{C'B}{}^{*} \begin{bmatrix} Z_g^{ps}(f+f_1) & 0 \\ 0 & Z_g^{ps*}(-f+f_1) \end{bmatrix} \mathbf{T}_{C'B} \quad \text{with } \mathbf{T}_{C'B} = \frac{1}{\sqrt{2}} \begin{bmatrix} \cos\theta - j\sin\theta & \sin\theta + j\cos\theta \\ \cos\theta + j\sin\theta & \sin\theta - j\cos\theta \end{bmatrix}, \tag{1}$$

where $\mathbf{T}_{C'B}$ is the complex transformation and angle transformation matrix, $\mathbf{T}_{C'B}{}^{*}$ is its conjugate transpose [24, 29], and Z_g^{ps*} is the conjugate of Z_g^{ps}. The converter-side scan measures the *dq* admittance matrix of the converter as

$$\mathbf{Y}_c^{dq}(f) = \begin{bmatrix} Y_{d,d}(f) & Y_{d,q}(f) \\ Y_{q,d}(f) & Y_{q,q}(f) \end{bmatrix} \text{ with } Y_{j,k}(f) = \frac{I_j(f)}{V_k(f)}, \tag{2}$$

where $j,k \in [d,q]$. For I and V, the subscript indicates the measured axis and k additionally indicates the perturbed axis. Further details are given in [23].

3) αβ-Frame Frequency Scanning

The *αβ*-scan extracts the small-signal transfer functions that relate the input currents (voltages) to the output voltages (currents) in the stationary *αβ* reference frame. With the exception of the transformations, the procedure is equivalent to the one described for the *dq*-scan.

The grid-side impedance in *αβ*-frame can be transformed from the phasor-domain-scan via

$$\mathbf{Z}_g^{\alpha\beta}(f) = \mathbf{T}_{C'}{}^{*} \begin{bmatrix} Z_g^{ps}(f) & 0 \\ 0 & Z_g^{ps*}(-f) \end{bmatrix} \mathbf{T}_{C'} \quad \text{with } \mathbf{T}_{C'} = \frac{1}{\sqrt{2}} \begin{bmatrix} 1 & j \\ 1 & -j \end{bmatrix}, \tag{3}$$

where $\mathbf{T}_{C'}$ is the complex transformation matrix [29]. The converter-side scan measures the *αβ* admittance of the converter as

$$\mathbf{Y}_c^{\alpha\beta}(f) = \begin{bmatrix} Y_{\alpha,\alpha}(f) & Y_{\alpha,\beta}(f) \\ Y_{\beta,\alpha}(f) & Y_{\beta,\beta}(f) \end{bmatrix} \text{ with } Y_{j,k}(f) = \frac{I_j(f)}{V_k(f)}, \tag{4}$$

where $j,k \in [\alpha,\beta]$. For I and V, the subscript indicates the measured axis and k additionally indicates the perturbed axis.

C. Stability Analysis

Depending on the reference frame of the impedance model, different stability analysis methods can be used. This section highlights the main differences.

1) Stability Analysis for Positive-Sequence SISO Model

The positive sequence impedance model of the system can be analyzed via the Bode plot and the Nyquist plot.

The Bode plot uses both impedances, $Z_g^{ps}(f)$ and $Z_c^{ps}(f)$, to estimate the phase and gain margins as well as the oscillation

frequency [30].

For the Nyquist stability criterion, the impedance ratio, i.e., $L(f) = Z_g^{ps}(f)Y_c^{ps}(f)$, is regarded as the open-loop gain of the system, as shown in Fig. 1. The Nyquist plot can be used to evaluate the phase and gain margins, and to determine the oscillation frequency of an unstable system.

2) Stability Analysis for dq- and αβ-Frame MIMO Models

For the dq- and $\alpha\beta$-frame impedance models, the system stability can be assessed via multi-variable impedance modeling and analysis methods [25, 31]. The impedance ratio of the grid impedance and the converter admittance transfer matrices is defined as $\mathbf{L}(f) = \mathbf{Z}_g(f)\mathbf{Y}_c(f)$ and can be regarded as the open-loop gain of the system, as shown in Fig. 1. The eigenloci of **L** can be analyzed via the generalized Nyquist criterion (GNC) [23]. The system is stable if, and only if, the net sum of the counter-clockwise encirclements of the critical point by the set of eigenloci of **L** equals the total number of right-half plane poles of **L** [32]. Furthermore, if the transfer matrices of converter and grid subsystem do not have any uncontrollable or unobservable (open-loop) modes in the right-half plane, meaning that they are individually stable, the system is stable if the eigenloci of **L** do not encircle the critical point. This is the case for many practical system scenarios, where the grid subsystem is stable without the connection of the converter subsystem, and the converter subsystem is stable when it is connected to an ideal voltage source [14]. The frequency at the crossing with the unit circle indicates the oscillation frequency for the unstable system and the phase margin.

III. Key Aspects of Scanning Techniques

TABLE I summarizes and compares the key aspects of the previously described scanning techniques, the extracted models, and their stability analysis.

The scanning methods should be used with their respective stability criterion to provide reliable prediction results. In this paper, the Nyquist diagram is used for stability assessment. Since the dq and $\alpha\beta$-scans provide a two-dimensional model, two sets of eigenloci are analyzed. Under such circumstances, instability is confirmed if at least one eigenlocus, in the following called the dominant eigenlocus, fulfills the criterion introduced in Section II.C.2). The stability margins and oscillation frequency should be evaluated based on the dominant eigenlocus of **L**. Hence, due to its lower dimension, stability assessment using the positive-sequence impedance is easier and faster.

The reliability of different scanning methods mainly depends on the accuracy of the associated Nyquist diagrams, especially where they approach the critical point. For the ps-scan, the prediction reliability depends on the accuracy of the impedance ratio for a range of frequencies. For the dq and $\alpha\beta$ scans, the reliability depends on the accuracy of the eigenvalues of **L** for a range of perturbation frequencies. Furthermore, as derived in [24], dq impedance models can capture dq coupling occurring in control systems of certain grid components. For such systems, sequence and $\alpha\beta$-scans usually exhibit an error, which may lead to erroneous predictions in critical cases.

The scan parameters such as the perturbation amplitude and the DFT window size can significantly affect the accuracy of the impedances, and thus play an important role in the reliability of the scans. The perturbation amplitude should be as high as possible but may not excite non-linearities and saturation effects. A perturbation amplitude of 0.01 p.u. is used for the perturbation signals in this paper.

The Nyquist diagrams can be used to estimate the frequency of oscillations in unstable cases. If the ps-scan is used, the frequency at which the Nyquist diagram of the ps-impedance-ratio intersects with the unit circle gives an estimate of the oscillation frequency. If the dq and $\alpha\beta$-scans are used, the frequency at which the dominant eigenlocus of **L** intersects with the unit circle provides indicates the oscillation frequency.

The computational burden is another important aspect of the measurement-based scanning methods. The time-domain EMT simulations used for the frequency scanning of the converter subsystem imposes a significant computational burden and is the main contributor to computation time. Furthermore, the larger the frequency range of interest and the higher the frequency resolution, the higher the number of simulations that need to be performed. Due to their little contribution, the phasor-domain scanning of passive grid subsystems, the post processing, and execution of stability assessment scripts can be neglected when assessing the computational speed.

For the ps-scan, a single simulation run is required for each frequency. However, for the dq and $\alpha\beta$-scans, two separate simulation runs are required to yield the impedance parameters for each frequency. Hence, the total number of simulations per subsystem is twice that of the ps-scan. An exception is the dq-

TABLE I: Key Aspects of Different Scanning Techniques

Item	ps-scan		dq-scan	$\alpha\beta$-scan
Stability criterion	Bode plot	Nyquist criterion	Generalized Nyquist criterion	Generalized Nyquist criterion
Parameter	$Z_g^{ps}(f)$ and $Z_c^{ps}(f)$	$L(f)$	$\mathbf{L}(f)$ in dq-frame	$\mathbf{L}(f)$ in $\alpha\beta$-frame
Prediction reliability	Good, Depends on impedance model accuracy	Good, Depends on impedance ratio accuracy	Very good, captures dq coupling Depends on eigenvalue accuracy	Good Depends on eigenvalue accuracy
Stability margin	yes, visualized	yes	yes	yes
Oscillation frequency	Magnitude intersection	intersectionwith the unit circle	intersection of dominant eigenlocus with the unit circle	intersection of dominant eigenlocus with the unit circle
Computational burden	Lowest		Generally, 2 × equivalent ps-scan Here, equal to equivalent ps-scan	2 × equivalent ps-scan

scan for the specific frequency range $[0, f_1]$. By transformation from *dq*- to positive- and negative sequence, and subsequent transformation of the negative-sequence portion to positive sequence, the *dq*-scan yields a ps-impedance for the frequency range $[0, 2f_1]$. Therefore, in this specific case the number of simulations required for ps- and *dq*-scan are equal.

It should be noted that this is a rough estimation of the computation time. The computation of additional transformations and signal processing in the MIMO scans lead to a higher computational burden. Furthermore, convergence times might vary for the three methods.

IV. Simulation Results

A. Implementation of Frequency Scanning Techniques

The frequency scanning techniques have been implemented in EMTP [33]. The simulation time step is 50 µs, and the maximum simulation time is 100 s. The initial perturbation amplitude is 1 % of the nominal voltage at the POI regardless of the scanning technique. The DFT window size is 1 s. The results of the frequency scans are saved in datasets for offline post-processing and stability assessment in MATLAB. It should be noted that phasor-domain scanning was used for the ps-scan of the grid subsystems.

B. System Under Study & Study Cases

Two cases have been investigated that exhibit super- and sub-synchronous controller interactions with FSC and DFIG WPs. The single-line diagram of the system for the test cases is depicted in Fig. 4. This test system is adopted from [5] where the WP is connected to high-voltage networks via two parallel transmission lines. After a fault, the circuit breakers (CBs) are opened, leaving the WP radially connected to Line 1.

- Case I: FSC wind turbines are employed, and super-synchronous oscillations emerge after the contingency.
- Case II: DFIG wind turbines are employed, and sub-synchronous oscillations emerge after the contingency.

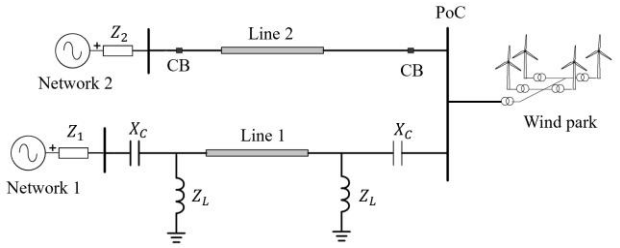

Fig. 4: The single-line diagram of the benchmark systems

The nominal system frequency is 60 Hz. The transmission networks operate at the rated voltage of 500 kV, with the equivalent impedances $Z_1 = Z_2 = 7.5 + j75\ \Omega$. Lines 1 and 2 are distributed constant parameter models. The shunt reactors Z_L each provide 230 MVAr reactive power (75 % shunt compensation), while the series capacitor banks X_C at the ends of line 1 are employed for a series compensation level of 50 %. The major WP and line parameters are given in TABLE II.

TABLE II: Simulation parameters of transmission lines and WPs

	Parameter	Value
Line	Length of Line 1 (km)	500
	Length of Line 2 (km)	100
	Resistance (Ω/km)	0.0283
	Inductance (Ω/km)	0.3244
	Charging capacitance (µS/km)	5.0512
WP	Number of wind turbines	400
	Wind turbine rated power (MW)	1.5
	Rated power of wind turbines (MVA)	1.667
	Rated power of turbine transformer (MVA)	1.75
	Rated power of the park transformer (MVA)	675
	Rated voltage of the turbine (kVRMSLL)	0.575
	Rated voltage the collector (kVRMSLL)	34.5
	DC voltage (V)	575×2
	Resistance of the choke filter (p.u.)	5×10^{-3}
	Inductance of the choke filter (p.u.)	0.5
	Reactive power of harmonic filter (kVAr)	75
FSC	Grid-side converter rise time (ms)	6
	Machine-side converter rise time (ms)	20
	DC time constant (ms)	150
	Prop. gain of the voltage regulator	2
	wind speed (m/s)	11.2
DFIG	Grid-side converter rise time (ms)	10
	Rotor-side converter rise time (ms)	20
	Prop. Gain of rotor-side V control	2
	Prop. Gain of rotor-side P control	1
	Integral gain of rotor-side P control	10
	wind speed (m/s)	9

C. Results

As demonstrated in Fig. 5, the tripping of Line 2 leads to significant oscillations. In case I, the super-synchronous oscillation at 85.6 Hz is dominant while a mirrored coupling frequency can be observed at 22 Hz. In case II, there is a sub-synchronous oscillation at 26 Hz, and no significant complementary frequency is observed.

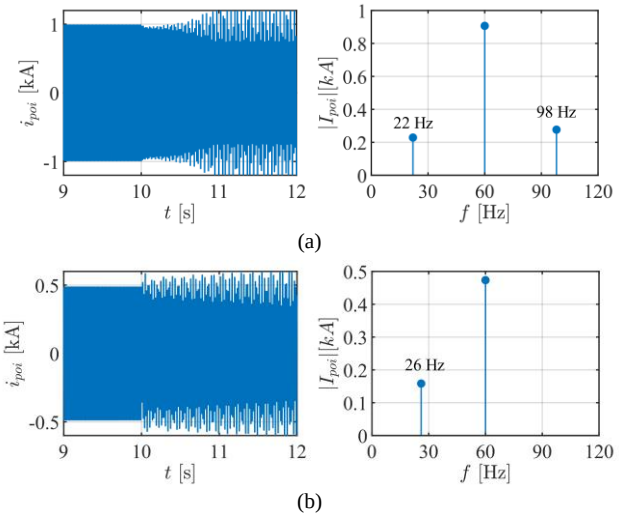

Fig. 5: Snapshots of the current measured at the POI before and after the contingency. Line 2 trips at t = 10 s (a): Case I (b): Case II

The Nyquist diagrams are depicted in Fig. 6
(b)

Fig. 6-Fig. 8. The eigenloci of all scans encircle the critical point (✳-marker). Furthermore, the eigenlocus of the ps-scan and the dominant eigenlocus of the *αβ*-scan are virtually equal with minor differences due to the scanning procedure.

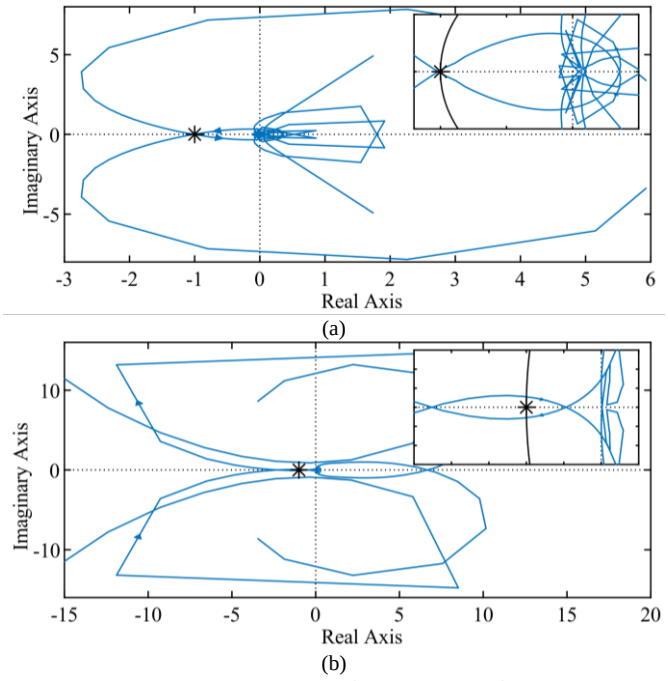

Fig. 6: The Nyquist diagrams obtained from the ps-scan for unstable cases: (a) Case I (b) Case II

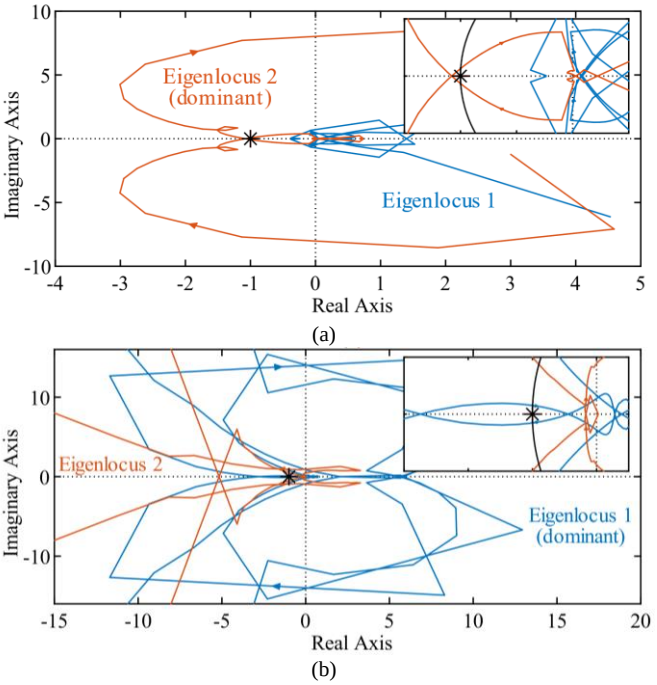

Fig. 7: The Nyquist diagrams based on the *dq*-scan for unstable cases: (a) Case I (b) Case II

Moreover, the results reveal that a change of the wind turbine model or wind speed leads to substantially different eigenloci even though both cases have the same grid-side impedance. In addition, the Nyquist diagrams for stable cases (not presented here due to page limit) confirm stability with relatively large margins. It is concluded that either of the frequency scanning techniques in conjunction with the Nyquist criterion can reliably assess the system's stability.

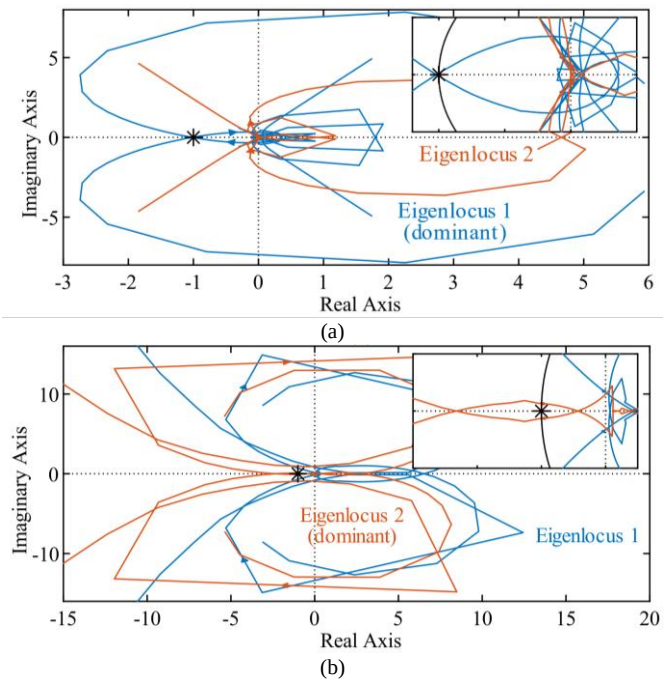

Fig. 8: The Nyquist diagrams based on the $\alpha\beta$-scan for unstable cases: (a) Case I (b) Case II

TABLE III compares the estimated oscillation frequencies. The estimates for case II are sufficiently accurate, regardless of the reference frame. For case I, however, the *dq*-scan is sufficiently accurate, while the others exhibit an error of 3 Hz. The results indicate that the *dq*-scan provides better estimates of the oscillation frequency when the WP employs FSC wind turbines. This can be attributed to the fact that MIMO impedance models in *dq*-frame capture mirror frequency coupling [24], whereas SISO models and the MIMO $\alpha\beta$-frame impedance models do not.

TABLE IV shows the phase and gain margins derived from the Nyquist diagrams. The phase margins for all diagrams are very small, especially in case II. Furthermore, the gain margins are also very small for case I. In fact, small changes in grid-side converter rise time may make the system critically stable.

TABLE III: ESTIMATION OF THE OSCILLATION FREQUENCY FOR THE UNSTABLE CASES

Case	Oscillation frequency (Hz)			
	ps-scan	*dq*-scan	$\alpha\beta$-scan	DFT of the POI current
I	101	97.5	101	98.0
II	26.3	26.2	26.3	26.0

TABLE IV: STABILITY MARGIN ESTIMATION USING SCANNING TECHNIQUES FOR THE UNSTABLE CASES

Case	ps-scan		*dq*-scan		$\alpha\beta$-scan	
	Phase margin (deg)	Gain margin (dB)	Phase margin (deg)	Gain margin (dB)	Phase margin (deg)	Gain margin (dB)
I	-0.76	-0.16	-3.87	-0.66	-0.76	-0.16
II	-3.13	+6.51 -7.12	-4.38	+6.97 -8.8	-3.78	+7.2 -7.36

The simulation times for frequency scanning of the converter subsystem are given in TABLE V. The ps-scan is the computationally fastest technique, and the *αβ*-scan is the slowest with more than two times the simulation time of the ps-scan for case II. For case I, however, the difference is much more pronounced. The simulation time of the *dq*-scan is a slightly more than for the ps-scan in both cases.

In principle, the simulation time should be proportional to the amount of performed scans. Therefore, one might assume that *dq* and *αβ*-scans have twice the simulation time of the ps-scan, since the two axes need to be perturbed separately. However, for the frequency range of interest in this paper, i.e., 1-120 Hz, the *dq*-scan only needs to be performed for the range 1-60 Hz, which can be transformed to 1-120 Hz in positive-sequence. The oscillation frequency and its complementary frequency can be found by simply adding and subtracting the fundamental frequency from the oscillation frequency found in the *dq*-analysis. Therefore, the number of scans required for ps and *dq*-scan are equal for this specific frequency range. The *αβ*-scan requires twice the number of scans for the given frequency range. The results support this reasoning, with the exception of the *αβ*-scan for case I.

Deviations in the actual simulation time from these simplified assumptions can be explained by

1. differences in actual computation time for each scan depending on the operation point and resulting numeric calculations.
2. additional mathematical operations due to the signal processing of two axes for *dq* and *αβ*-scans, compared to one axis for the ps-scan.
3. variation of the computation power of the simulation hardware.

The given simulation time should, therefore, be regarded as approximate indication only.

TABLE V: CPU SIMULATION TIME FOR SCANNING OF THE WP SUBSYSTEM

Case	CPU time (s)				
	ps-scan	*dq*-scan		*αβ*-scan	
		d axis	*q* axis	*α* axis	*β* axis
	1-119 Hz	1-59 Hz	1-59 Hz	1-119 Hz	1-119 Hz
I	1565	811	903	4517	4909
II	1667	957	986	1742	1698

V. CONCLUSION

This paper presents the use of frequency scanning in conjunction with EMT simulations to extract frequency-dependent impedance models of power systems and wind parks. The impedance models can be analyzed via the Nyquist diagram to predict control interactions between wind parks and the grid, extract the frequency of oscillation, and evaluate stability margins.

This article presents a comparison of frequency scanning techniques in positive-sequence, *dq*, and *αβ*-frame. The techniques are tested on two unstable grid cases, featuring FSC and DFIG wind parks. Stability assessment of the resulting impedance models is performed to compare the techniques. Furthermore, the computational efficiency is investigated.

The results corroborate that sub- and super-synchronous oscillations can be detected using either reference frame for the impedance model. The *dq*-scan is more accurate in the estimation of the oscillation frequency for FSC-based wind parks. It is shown that the positive-sequence scan has the fastest simulation time. In this special case, i.e., for a frequency range of interest of 1-120 Hz, the computational burden of the *dq*-scan is much lower than the *αβ*-scan, and close to the positive-sequence scan.

VI. REFERENCES

[1] H. Holttinen and et al., "Variable Renewable Energy Integration: Status Around the World," *IEEE Power and Energy Magazine,* vol. 19, no. 6, pp. 86-96, 2021.

[2] S. D. Ahmed and et al., "Grid Integration Challenges of Wind Energy: A Review," *IEEE Access,* vol. 8, pp. 10857-10878, 2020.

[3] IEEE PES Task Force, "Wind Energy Systems Sub-Synchronous Oscillations: Events and Modeling," IEEE Technical Report, 2020.

[4] M. Liserre, R. Teodorescu and F. Blaabjerg, "Stability of photovoltaic and wind turbine grid-connected inverters for a large set of grid impedance values," *IEEE Transactions on Power Electronics,* vol. 21, no. 1, pp. 263-272, 2006.

[5] U. Karaagac, J. Mahseredjian, S. Jensen, R. Gagnon, M. Fecteau and I. Kocar, "Safe Operation of DFIG-Based Wind Parks in Series-Compensated Systems," *IEEE Transactions on Power Delivery,* pp. 709-718, 2018.

[6] F. Zhang, L. Cheng, W. Gao and R. Huang, "Synchrophasors-Based Identification for Subsynchronous Oscillations in Power Systems," *IEEE Transactions on Smart Grid ,* vol. 10, no. 2, pp. 2224-2233, 2019.

[7] A. S.Trevisan and et al., "Analysis of low frequency interactions of DFIG wind turbine systems in series compensated grids," *Electric Power Systems Research,* vol. 191, 2021.

[8] L. Fan, "Modeling Type-4 Wind in Weak Grids," *IEEE Transactions on Sustainable Energy ,* vol. 10, no. 2, pp. 853-864, 2019.

[9] T. Zhang, Z. Hao, J. Shu, Y. Zhao and S. Yuan, "Research on SSO Suppression of DFIG-Based Wind Farm by Impedance Scanning," in *IEEE Power & Energy Society General Meeting (PESGM),* Montreal, 2020.

[10] C. Zhang, M. Molinas, A. Rygg and X. Cai, "Impedance-Based Analysis of Interconnected Power Electronics Systems: Impedance Network Modeling and Comparative Studies of Stability Criteria," *IEEE Journal of Emerging and Selected Topics in Power Electronics,* vol. 8, no. 3, pp. 2520-2533, 2020.

[11] A. S. Trevisan and et al., "Field Validated Generic EMT-Type Model of a Full Converter Wind Turbine Based on a Gearless Externally Excited Synchronous Generator," *IEEE Transactions on Power Delivery,* vol. 33, no. 5, pp. 2284-2293, 2018.

[12] S. Shah and et al., "Impedance Methods for Analyzing Stability Impacts of Inverter-Based Resources: Stability Analysis Tools for Modern Power Systems," *IEEE Electrification Magazine ,* vol. 9, no. 1, pp. 53 - 65, 2021.

[13] J. Sun, "Small-Signal Methods for AC Distributed Power Systems-A Review," *IEEE Transactions on Power Electronics,* vol. 24, no. 11, pp. 2545-2554, 2009.

[14] J. Sun, "Impedance-Based Stability Criterion for Grid-Connected Inverters," *IEEE Transactions on Power Electronics,* vol. 26, no. 11, pp. 3075-3078, 2011.

[15] J. Sun, "Frequency-Domain Stability Criteria for Converter-Based Power Systems," *IEEE Open Journal of Power Electronics,* vol. 3, no. March, pp. 222-254, 2022.

[16] X. W. Yicheng Liao, "General Rules of Using Bode Plots for Impedance-Based Stability Analysis," in *IEEE 19th Workshop on Control and Modeling for Power Electronics, COMPEL 2018*, Padova, 2018.

[17] H. L. Jian Sun, "Sequence Impedance Modeling of Modular Multilevel Converters," *IEEE Journal of Emerging and Selected Topics in Power Electronics,* vol. 5, no. 4, pp. 1427-1443, 2017.

[18] P. G. B. L. Y. L. H. G. Shaojian Song, "Impedance Modeling and Stability Analysis of DFIG-Based Wind Energy Conversion System Considering Frequency Coupling," *Energies,* vol. 14, no. 11, p. 3243, 2021.

[19] A. M. G. Xiao Jiang, "A frequency scanning method for the identification of harmonic instabilities in HVDC systems," *IEEE Transactions on Power Delivery,* vol. 10, no. 4, pp. 1875-1881, 1995.

[20] P. K. V. G. R. W. Shahil Shah, "Sequence Impedance Measurement of Utility-Scale Wind Turbines and Inverters – Reference Frame, Frequency Coupling, and MIMO/SISO Forms," *IEEE Transactions on Energy Conversion,* vol. 37, no. 1, pp. 75-86, 2022.

[21] M. Cespedes and J. Sun, "Impedance Modeling and Analysis of Grid-Connected Voltage-Source Converters," *IEEE Transactions on Power Electronics,* vol. 29, no. 3, pp. 1254-1261, 2014.

[22] E. L. Wei Ren, "A Refined Frequency Scan Approach to Sub-Synchronous Control Interaction (SSCI) Study of Wind Farms," *IEEE Transactions on Power Systems,* vol. 31, no. 5, pp. 3904-3912, 2016.

[23] A. S. Trevisan, Â. Mendonça, R. Gagnon, J. Mahseredjian and M. Fecteau, "Analytically Validated SSCI Assessment Technique for Wind Parks in Series Compensated Grids," *IEEE Transactions on Power Systems,* vol. 36, no. 1, pp. 39 - 48, 2021.

[24] A. Rygg, M. Molinas, C. Zhang and X. Cai, "A Modified Sequence-Domain Impedance Definition and Its Equivalence to the dq-Domain Impedance Definition for the Stability Analysis of AC Power Electronic Systems," *IEEE Journal of Emerging and Selected Topics in Power Electronics,* vol. 4, no. 4, pp. 1383-1396, 2016.

[25] X. Wang, L. Harnefors and F. Blaabjerg, "Unified Impedance Model of Grid-Connected Voltage-Source Converters," *IEEE Transactions on Power Electronics,* vol. 33, no. 2, pp. 1775 - 1787, 2018.

[26] M. Lwin, R. Kazemi and D. Howard, "Frequency Scan Considerations for SSCI Analysis of Wind Power Plants," in *IEEE Power & Energy Society General Meeting (PESGM)*, Atlanta, 2019.

[27] S. Shah and et al., "Sequence Impedance Measurement of Utility-Scale Wind Turbines and Inverters Reference Frame, Frequency Coupling, and MIMO/SISO Forms," *IEEE Transactions on Energy Conversion*, pp. 1-12, 2021.

[28] B. L. Agarwal and R. G. Farmer, "Use of Frequency Scanning Techniques for SubsynchronousResonance Analysis," *IEEE Trans. Power Appar. Syst.,* Vols. PAS-98, no. 2, pp. 341-349, 1979.

[29] G. C. Paap, "Symmetrical Components in the Time Domain andTheir Application to Power Network Calculations," *IEEE Transactions on Power Systems,* vol. 15, no. 2, pp. 522-528, 2000.

[30] Y. Liao and X. Wang, "General Rules of Using Bode Plots for Impedance-Based Stability Analysis," in *IEEE 19th Workshop on Control and Modeling for Power Electronics*, Padua, 2018.

[31] J. Sun, "Impedance-Based Stability Criterion for Grid-Connected Inverters," *IEEE Transactions on Power Electronics* , vol. 26, no. 11, pp. 3075-3078, 2011.

[32] A. G. J. MacFarlane and I. Postlethwaite, "The generalized Nyquist stability criterion and multivariable root loci," *International Journal of Control,* vol. 25, no. 1, pp. 81-127, 1977.

[33] J. Mahseredjian and et al., "On a new approach for the simulation of transients in power systems," *Electric Power Systems Research,* vol. 77, no. 11, pp. 1514-1520, 2007.

[34] B. Wen, D. Boroyevich, R. Burgos, P. Mattavelli and Z. Shen, "Small-Signal Stability Analysis of Three-Phase AC Systems in the Presence of Constant Power Loads Based on Measured d-q Frame Impedances," *IEEE Transactions on Power Electronics,* vol. 30, no. 10, pp. 5952-5963, 2015.

[35] S. Shah and L. Parsa, "Impedance-Based Prediction of Distortions Generated by Resonance in Grid-Connected Converters," *IEEE Transactions on Energy Conversion,* vol. 34, no. 3, pp. 1264 - 1275, 2019.

[36] S. Shah, P. Koralewicz, V. Gevorgian, R. Wallen, K. Jha, D. Mashtare, R. Burra and L. Parsa, "Large-Signal Impedance-Based Modeling and Mitigation of Resonance of Converter-Grid Systems," *IEEE Transactions on Sustainable Energy,* vol. 10, no. 3, pp. 1439 - 1449, 2019.

[37] W. Stevenson and J. Grainger, "Symmetrical Components and Sequence Networks," in *Power System Analysis*, Singapore, McGraw-Hill, 1994, pp. 416-422.